

31. We thank L. C. Bonser, J. S. R. Dunlop, A. H. Hickman, M. van Kranendonk, the Geological Survey of Western Australia, P. van Loenhout, and Mount Magnet Drilling for assistance with core recovery; the NASA Astrobiology Drilling Program and NSF Geobiology and Low Temperature Geochemistry for funding; and

A. H. Knoll, J. Farquhar, R. E. Summons, and T. W. Lyons for advice.

Supporting Online Material

www.sciencemag.org/cgi/content/full/323/5917/1045/DC1
Materials and Methods

Figs. S1 and S2
Table S1
References

9 September 2008; accepted 6 January 2009
10.1126/science.1165675

Zircon Dating of Oceanic Crustal Accretion

C. Johan Lissenberg,^{1,2*†} Matthew Rioux,³ Nobumichi Shimizu,² Samuel A. Bowring,³ Catherine Mével¹

Most of Earth's present-day crust formed at mid-ocean ridges. High-precision uranium-lead dating of zircons in gabbros from the Vema Fracture Zone on the Mid-Atlantic Ridge reveals that the crust there grew in a highly regular pattern characterized by shallow melt delivery. Combined with results from previous dating studies, this finding suggests that two distinct modes of crustal accretion occur along slow-spreading ridges. Individual samples record a zircon date range of 90,000 to 235,000 years, which is interpreted to reflect the time scale of zircon crystallization in oceanic plutonic rocks.

Nearly two-thirds of Earth's crust is formed at mid-ocean ridges. Crustal growth is controlled by the transfer of melt from the mantle to the crust. There has been extensive research on the rates and volume of extrusive volcanism, but the time scales of melt delivery from the mantle and the resulting patterns of intrusive magmatism in these settings are not well known. This is largely because of the inaccessibility of lower crustal sections and the limited spatial resolution of indirect methods such as seismic imaging.

Recently, U-Pb geochronology of samples from exposed lower crustal sections has begun to constrain the timing of intrusive magmatism beneath mid-ocean ridge spreading centers. Previous studies, from Atlantis Bank on the Southwest Indian Ridge (1) and Atlantis Massif on the Mid-Atlantic Ridge (2), used ion microprobe U-Pb geochronology of zircon to date the crystallization of igneous rocks intruded into the lower crust in these areas. These studies have provided considerable new insight into the time scales of magmatism at mid-ocean ridges, presenting evidence for protracted lower crustal growth, but the relatively low precision of ion microprobe spot analyses [1.5 to 43%, 2σ (1)] and the complex tectonic histories of these areas limit our understanding of magmatic processes at typical slow-spreading ridge segments.

We report chemical abrasion–thermal ionization mass spectrometry [CA-TIMS (3)] U-Pb zircon dates from the Vema lithospheric section (VLS), located at 11°N on the Mid-Atlantic Ridge. The single-grain CA-TIMS dates have an uncertainty of 0.07 to 0.79% (2σ), which corresponds to an error of ~10,000 to 106,000 years, more than an order of magnitude more precise than published ion microprobe dates on similar-age oceanic gabbros.

The VLS is exposed along the transverse ridge of the Vema Fracture Zone, which rises to ~450 m below sea level, and comprises litho-

sphere that was uplifted ~10 to 11 million years ago (Ma) as a result of plate flexure (4), thus exposing a full section of mantle peridotites, lower crustal gabbros, and basaltic upper crust formed along the Mid-Atlantic Ridge (Fig. 1). The studied samples come from a narrow (6 km) section of the VLS centered around 42°42'W (Fig. 1), which formed at ~13 Ma according to plate motion models (5). The crustal section exposed along the VLS in the study area represents the northern end of an ancient ridge segment ~60 km in length [the EMAR segment of (4, 6)], and the section is thin [~2.2 km (7)] relative to the off-axis trace of the ancient segment center to the south (6). The crustal section, including the lower crust, is continuous, and is not composed of gabbro plutons intruding mantle peridotites, unlike the commonly inferred composition of slow-spreading segment ends (8). Gabbros exposed along the VLS in the study area commonly contain Fe-Ti oxides, indicating extensive differentiation.

We obtained U-Pb dates of 31 zircon grains and grain fragments separated from five gabbroic samples that were collected by submersible craft and by dredging along the VLS (7, 9) (see supporting online material for sample descriptions, analytical techniques, and data). Individual zircon dates range from 13.75 to 13.25 Ma (Fig. 2) and show a good correlation with sample location

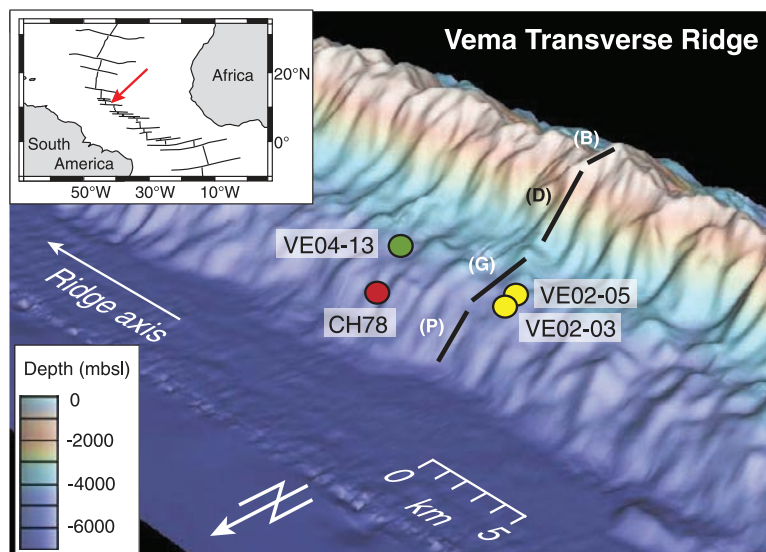


Fig. 1. Location of samples dated in this study. Inset shows location of VLS within the Atlantic Ocean. Schematic geological section of the VLS (black solid lines) after (7). Samples with prefix VE were sampled by the submersible Nautilie during the VemaNaute cruise (7, 9); samples with prefix CH were dredged during Jean Charcot Leg 78. On the basis of valley patterns observed in bathymetry, we estimate an along-axis uncertainty of 2 km for provenance of the dredged samples. P, peridotite; G, gabbro; D, dikes; B, basalt; mbsl, meters below sea level.

¹Equipe de Géosciences Marines, Institut de Physique du Globe de Paris, 4 Place Jussieu, 75252 Paris Cedex 05, France.

²Woods Hole Oceanographic Institution, Woods Hole, MA 02543, USA. ³Department of Earth, Atmospheric, and Planetary Sciences, Massachusetts Institute of Technology, Cambridge, MA 02139, USA.

*Present address: School of Earth and Ocean Sciences, Cardiff University, Park Place, Cardiff CF10 3YE, UK.

†To whom correspondence should be addressed. E-mail: lissenbergcj@cardiff.ac.uk

(Fig. 3). The youngest zircon grains of each of the samples define a half-spreading rate of 15.8 ± 1.6 mm/year (Fig. 3), in agreement with the rate of 16.1 mm/year predicted by plate motion models (5).

Each sample has single-grain zircon dates that span 90,000 to 235,000 years, rather than a single population with equivalent dates (Fig. 2). Our interpretation is that these ranges reflect the time

scale of zircon crystallization in mid-ocean ridge plutonic systems. In the dated gabbros, some zircons are included in amphibole (secondary after pyroxene) and plagioclase, whereas others occur along grain boundaries (fig. S1), consistent with an extended history of zircon growth. Individual zircon dates may therefore represent either discrete events or an average of a crystallization interval (with each grain capturing

different parts of the growth history). As a result, the observed range in dates represents a minimum time scale of gabbro crystallization.

The Ti-in-zircon thermometer (10, 11) indicates that zircon in individual oceanic gabbros may crystallize over a temperature range of $\sim 60^\circ$ to 120°C (fig. S2) (12). If this is the case for our samples, the intersample range in zircon dates we obtained indicates that the Vema gabbros cooled at rates of $\sim 300^\circ$ to 1300°C per million years, consistent with thermochronology-derived cooling rates of 800°C per million years determined for slow-spreading lower crust (13).

The extended time scales of zircon crystallization are also consistent with seismic velocity anomalies at slow-spreading ridges. For the half-spreading rate of 15.8 mm/year defined by the zircon dates, the age span observed in the Vema samples would correspond to 1.4 to 3.7 km of spreading. At slow-spreading ridge segments, lower crustal negative velocity anomalies, signaling the presence of partial melt, extend up to ± 10 km across-axis (14, 15), although this may have been less for the VLS owing to its proximity to a transform fault.

An alternative interpretation is that the observed range in zircon dates may reflect the assimilation of slightly older adjacent plutonic rocks during intrusion and cooling, a process that is commonly seen in continental crust. The date of each grain would then represent a mixture of a slightly older core and a younger magmatic rim; the range for each sample would reflect varying amounts and/or age of inherited components. However, cathodoluminescence and electron backscatter images of zircon from each sample, including grains that were subsequently analyzed, show no evidence for core/rim overgrowths or sharp breaks in composition, as would be expected in this model (Fig. 4). Thus, we prefer the model for protracted growth of zircon during solidification of the gabbroic plutons.

Results from the VLS are distinct from dating studies at Atlantis Bank (1) and Atlantis Massif (2), which suggests that there may be at least two different mechanisms of oceanic crustal accretion. At the VLS, the linear progression of ages away from the ridge axis (Fig. 3), combined with the continuous nature of the lower crust and scarcity of gabbroic plutons in the mantle section (7), suggest that the crust formed by highly regular, ridge-centered, shallow delivery of melt. In contrast, the data from Atlantis Bank and Atlantis Massif document the presence of inherited cores of up to 1.5 million years older than corresponding rims, with zircon dates as much as 2.5 million years older than the predicted magnetic ages for a given volume of crust. This extended time span of crustal growth was attributed to crystallization of gabbros in the mantle at depths of up to 18 km, followed by uplift to lower crustal depths and renewed magmatism (1, 2). The different growth histories may relate to contrasting spreading histories. Atlantis Bank and Atlantis Massif expose sections of lower crust unroofed by low-angle

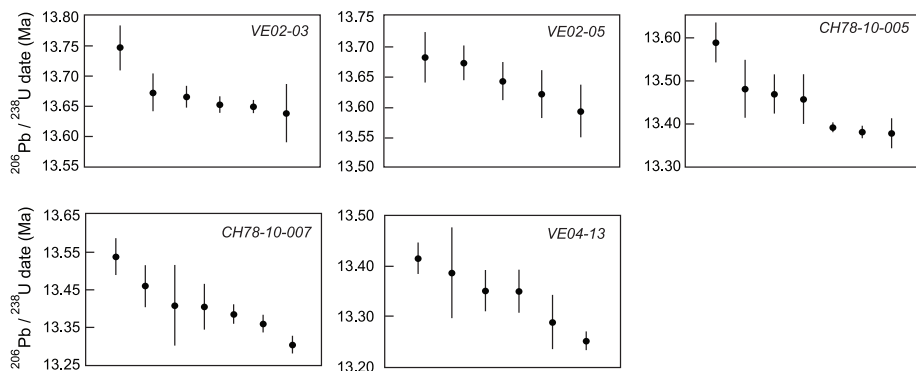


Fig. 2. CA-TIMS results for gabbros from the VLS. The single zircon grains (along the x axis) show a range in $^{206}\text{Pb}/^{238}\text{U}$ dates for each sample that exceeds the analytical uncertainties.

Fig. 3. $^{206}\text{Pb}/^{238}\text{U}$ dates of individual zircon crystals versus distance from the ridge axis. Half-spreading rate (defined by the youngest zircon in each of the samples) is shown by a gray line, with 2σ error envelope marked by dashed lines. Note that VE02-03 and VE02-05, as well as CH78-10-005 and CH78-10-007, were sampled from the same longitude but are separated by 300 m for clarity. There is a 2-km uncertainty in distance from the ridge axis for dredge samples CH78-10-005 and CH78-10-007. Grains for which common Pb exceeded 1 pg were excluded from the discussion (see supporting online material) and are shown in gray.

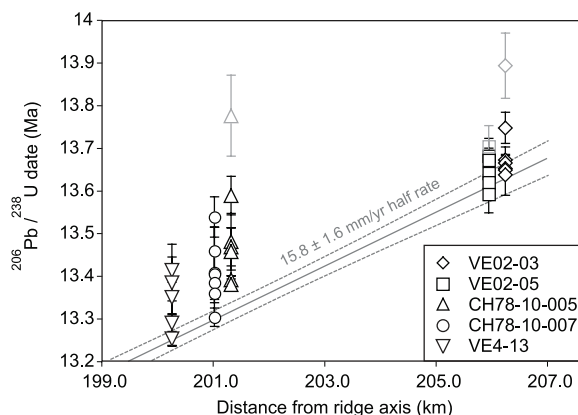
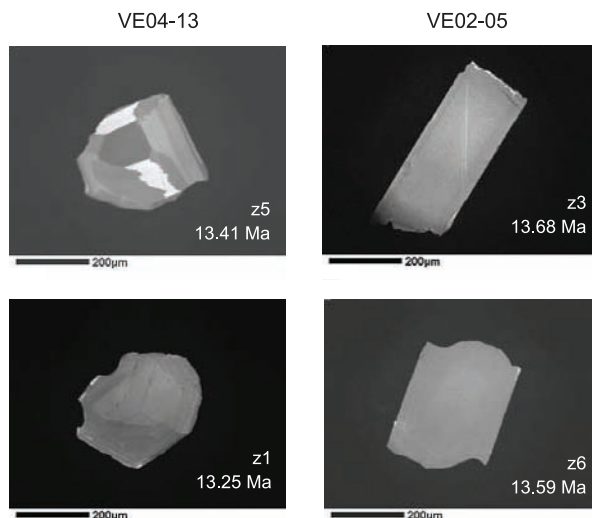


Fig. 4. Cathodoluminescence images of oldest and youngest zircon grains from Vema gabbros VE04-13 and VE02-05. Internal structures are consistent with growth during a single magmatic episode, lacking evidence for inherited cores overgrown by younger rims.



detachment faults [so-called oceanic core complexes (16–18)], typical of asymmetrically spreading ridge segments (19). The detachment faults are inferred to root in the lower crust or mantle beneath the ridge axis [e.g., (20, 21)]. This would lead to an axial thermal structure, and hence a pluton emplacement pattern, that deviates considerably from that of a regular, symmetrically spreading ridge segment. In addition, plutons may intrude as the lower crust is exhumed (22), potentially leading to the juxtaposition of gabbros with different ages. Detachment faulting may thus substantially influence crustal accretion, possibly explaining the range of gabbro ages seen in Atlantis Bank and Atlantis Massif. The Vema samples come from an intact crustal section devoid of detachment faults, and the regular pattern of crustal accretion and absence of anomalously old ages may be typical of symmetrical accretion at slow-spreading ridges.

References and Notes

1. J. J. Schwartz *et al.*, *Science* **310**, 654 (2005).
2. C. B. Grimes, B. E. John, M. Cheadle, J. L. Wooden, *Geochim. Geophys. Geosyst.* **9**, Q08012 (2008).

3. J. M. Mattinson, *Chem. Geol.* **220**, 47 (2005).
4. E. Bonatti *et al.*, *Earth Planet. Sci. Lett.* **240**, 642 (2005).
5. R. D. Müller *et al.*, *Geochem. Geophys. Geosyst.* **9**, Q04006 (2008).
6. E. Bonatti *et al.*, *Nature* **423**, 499 (2003).
7. J.-M. Auzende *et al.*, *Nature* **337**, 726 (1989).
8. M. Cannat, *J. Geophys. Res.* **101**, 2847 (1996).
9. J. M. Auzende *et al.*, *Campagne Vema-naute 13/8/1989–16/9/1989, Cruise Report* (1988).
10. E. Watson, D. Wark, J. Thomas, *Contrib. Mineral. Petrol.* **151**, 413 (2006).
11. J. Ferry, E. Watson, *Contrib. Mineral. Petrol.* **154**, 429 (2007).
12. Calculated using data of (23–25) for samples with more than three zircon grains analyzed.
13. B. E. John *et al.*, *Earth Planet. Sci. Lett.* **222**, 145 (2004).
14. R. A. Dunn, V. Lekić, R. S. Detrick, D. R. Toomey, *J. Geophys. Res.* **110**, B09101 (2005).
15. J. P. Canales, J. A. Collins, J. Escartin, R. S. Detrick, *J. Geophys. Res.* **105**, 2699 (2000).
16. J. R. Cann *et al.*, *Nature* **385**, 329 (1997).
17. D. K. Blackman, J. R. Cann, R. Janssen, D. K. Smith, *J. Geophys. Res.* **103**, 21315 (1998).
18. H. J. B. Dick *et al.*, *Proc. ODP Sci. Res.* **118**, 359 (1991).
19. J. Escartin *et al.*, *Nature* **455**, 790 (2008).
20. B. E. Tucholke, J. Lin, M. C. Kleinrock, *J. Geophys. Res.* **103**, 9857 (1998).

21. B. J. deMartin, R. A. Sohn, J. P. Canales, S. E. Humphris, *Geology* **35**, 711 (2007).
22. H. J. B. Dick, M. A. Tivey, B. E. Tucholke, *Geochem. Geophys. Geosyst.* **9**, Q05014 (2008).
23. B. Fu *et al.*, *Contrib. Mineral. Petrol.* **156**, 197 (2008).
24. L. A. Coogan, R. W. Hinton, *Geology* **34**, 633 (2006).
25. C. B. Grimes *et al.*, *Geology* **35**, 643 (2007).
26. Supported by a grant from the Woods Hole Oceanographic Institution Deep Ocean Exploration Institute (N.S., C.J.L.). U-Pb geochronology was supported in part by NSF grant OCE-0727914 (S.A.B.). We thank H. Dick for discussions, J. Honnorez for providing CH78 cruise information, and two anonymous reviewers for their comments. Figure 1 was made using GeoMapApp. This is IPGP contribution 2457.

Supporting Online Material

www.sciencemag.org/cgi/content/full/1167330/DC1
SOM Text
Figs. S1 to S4
Tables S1 and S2
References

17 October 2008; accepted 15 December 2008
Published online 29 January 2009;
10.1126/science.1167330
Include this information when citing this paper.

A Self-Regulatory System of Interlinked Signaling Feedback Loops Controls Mouse Limb Patterning

Jean-Denis Bénazet,¹ Mirko Bischofberger,² Eva Tiecke,¹ Alexandre Gonçalves,¹ James F. Martin,³ Aimée Zuniga,¹ Felix Naef,² Rolf Zeller^{1*}

Embryogenesis depends on self-regulatory interactions between spatially separated signaling centers, but few of these are well understood. Limb development is regulated by epithelial-mesenchymal (e-m) feedback loops between sonic hedgehog (SHH) and fibroblast growth factor (FGF) signaling involving the bone morphogenetic protein (BMP) antagonist Gremlin1 (GREM1). By combining mouse molecular genetics with mathematical modeling, we showed that BMP4 first initiates and SHH then propagates e-m feedback signaling through differential transcriptional regulation of *Grem1* to control digit specification. This switch occurs by linking a fast BMP4/GREM1 module to the slower SHH/GREM1/FGF e-m feedback loop. This self-regulatory signaling network results in robust regulation of distal limb development that is able to compensate for variations by interconnectivity among the three signaling pathways.

Tissue morphogenesis depends on self-regulatory mechanisms that buffer genetic and environmental variations. With the exception of self-regulatory bone morphogenetic

protein (BMP) signaling during gastrulation, the mechanisms endowing vertebrate development with robustness are largely unknown (1, 2). The vertebrate limb bud is a classical model to study organogenesis, and its development is driven by signaling interactions between two instructive centers (3, 4). The sonic hedgehog (SHH)/Gremlin1 (GREM1)/fibroblast growth factor (FGF) feedback loop (5–7) coordinates SHH signaling by the mesenchymal zone of polarizing activity (ZPA) with FGF signaling by the apical ectodermal ridge (AER) (4, 8–10). In *Grem1*-deficient mouse limb buds, this feedback loop is not established, which disrupts both signaling centers and distal development as revealed by fusion of ulna and radius

and loss of digits (Fig. 1A). Previous studies (5–7) suggested that GREM1-mediated antagonism of mesenchymal BMPs is key to SHH-mediated specification of digits 2 to 5 and proliferative expansion of the digit territory (autopod) (8, 10). Three BMP ligands are expressed in limb buds (fig. S1) (11), and genetic studies revealed that mesenchymal BMP signaling inhibits anterior expansion of *AER-Fgf* expression and polydactyly (formation of additional digits) (12, 13) and that a minimal BMP threshold is required to initiate chondrogenesis of posterior digits (14, 15).

To identify the BMP ligand(s) antagonized by GREM1, we performed a genetic interaction screen in mouse embryos. Halving the *Bmp2* or *Bmp7* gene dosage only slightly improved limb development (Fig. 1A), whereas inactivation of one *Bmp4* allele restored the zeugopod (ulna and radius) and the posterior-most digits (Fig. 1B) ($n = 24/24$). Complete inactivation of *Bmp7* resulted in similar restoration (fig. S2), which indicates that GREM1 may reduce overall BMP activity. Cross-regulation among BMP ligands is unlikely because genetic lowering of one *Bmp* did not alter the expression of the others (figs. S1 and S2). Hindlimb development was also restored, but we only show forelimbs because the molecular alterations in *Grem1*^{Δ/Δ} limb buds have been best characterized in forelimbs (5–7). In addition, the *Prx1*-Cre transgene was active in forelimb buds from an early stage.

Because genetic reduction of *Bmp4* in *Grem1*^{Δ/Δ} embryos was most potent, we used a hypomorphic floxed *Bmp4* allele (*Bmp4*^{h5}) (16) with decreased activity (fig. S1) to reduce the *Bmp4* gene dosage in a stepwise manner. In this allelic series, forelimb development was progressively restored with proximal-to-distal and posterior-to-anterior

¹Developmental Genetics, Department of Biomedicine, University of Basel, Mattenstrasse 28, CH-4058 Basel, Switzerland.

²Computational Systems Biology Group, Ecole Polytechnique Federale de Lausanne, Swiss Institute for Experimental Cancer Research and Swiss Institute of Bioinformatics, AAB 0 21 Station 15, CH-1015 Lausanne, Switzerland. ³Texas A&M Health Science Center, Institute of Biosciences and Technology, 2121 West Holcombe Boulevard, Room 907, Houston, TX 77030, USA.

*To whom correspondence should be addressed. E-mail: rolf.zeller@unibas.ch